

Geophysical Research Letters®

RESEARCH LETTER

10.1029/2024GL114047

Key Points:

- Alluvial ridges are spatially discontinuous landforms that occur in distinct segments along avulsing rivers
- Alluvial ridges exhibit a nested hierarchy of scales, from segments to complexes
- The length of the avulsion scales positively with alluvial ridge length

Supporting Information:

Supporting Information may be found in the online version of this article.

Correspondence to:

J. H. Gearon,
jake.gearon@gmail.com

Citation:

Gearon, J. H., & Edmonds, D. A. (2025). River avulsion precursors encoded in alluvial ridge geometry. *Geophysical Research Letters*, 52, e2024GL114047. <https://doi.org/10.1029/2024GL114047>

Received 2 DEC 2024

Accepted 7 APR 2025

Author Contributions:

Conceptualization: J. H. Gearon, D. A. Edmonds

Data curation: J. H. Gearon

Formal analysis: J. H. Gearon, D. A. Edmonds

Funding acquisition: D. A. Edmonds

Investigation: J. H. Gearon

Methodology: J. H. Gearon

Project administration: D. A. Edmonds

Resources: D. A. Edmonds

Software: J. H. Gearon

Supervision: D. A. Edmonds

Validation: J. H. Gearon

Visualization: J. H. Gearon

Writing – original draft: J. H. Gearon

Writing – review & editing: J. H. Gearon, D. A. Edmonds

© 2025. The Author(s).

This is an open access article under the terms of the [Creative Commons Attribution License](#), which permits use, distribution and reproduction in any medium, provided the original work is properly cited.

River Avulsion Precursors Encoded in Alluvial Ridge Geometry



J. H. Gearon¹ and D. A. Edmonds¹

¹Department of Earth & Atmospheric Sciences, Indiana University, Bloomington, IN, USA

Abstract River avulsions generate catastrophic floods that threaten communities, ecosystems, and infrastructure worldwide. Alluvial ridges—elevated regions of near-channel topography—are thought to precede avulsions, yet their spatial patterns and relationship to avulsion impact remain poorly understood. We analyzed pre-event topographic cross-sections from 14 rivers to quantify avulsion potential (Λ), a metric combining ridge height and slope relative to the channel. Our analysis reveals that Λ varies downstream and defines distinct alluvial ridge segments. We identify two characteristic length scales: a longer-wavelength complex ($\bar{L}_\lambda \approx 30$ km) composed of shorter ridge segments ($\bar{L}_C \approx 8$ km). Segments with $\Lambda \geq 2$ correspond to 73% of observed avulsion activity locations ($n = 37$). Avulsion activity length (L_A) scales linearly with L_C ; evidence that ridge geometry controls avulsion activity size. These characteristic scales define both the minimum downstream extent of potential impact zones (L_C) and the spacing between avulsion-prone reaches (L_λ), enabling improved hazard assessment.

Plain Language Summary River avulsions are sudden shifts in a river's course, often causing devastating floods. Predicting avulsions is crucial for mitigating flood risk, but our current understanding of their precursors is limited. This study examines alluvial ridges—elevated areas near river channels—as potential indicators of avulsion risk. By analyzing a suite of river topography data from globally distributed examples, we found that a metric called avulsion potential, which combines measurements of relative alluvial ridge height and slope, reveals distinct high-risk zones along rivers. These zones correlate strongly with future avulsion activity locations. Moreover, the size of these ridges appears to control the extent of future avulsion activity. This finding could improve flood hazard assessments, particularly in data-scarce regions.

1. Introduction

River avulsions generate some of the most consequential fluvial floods on Earth (Sinha, 2009; Slingerland & Smith, 1998). Yet, predicting their occurrence remains elusive because their precursors are incompletely understood. The set up to an avulsion happens through sediment deposition in and around the river that stores potential energy in the form of an alluvial ridge (Allen, 1965; Bridge, 1984; Fisk, 1944; Nicholas et al., 2018; Slingerland & Smith, 1998). The actual avulsion can be triggered by an event, like a flood, that breaches the alluvial ridge and unleashes the stored energy through avulsion flooding and sediment mobilization (Edmonds et al., 2016). Because triggering events are largely stochastic and generally cause avulsion only when the river is set up, a useful precursor is one that is related to the long-term set up conditions that promote sedimentation.

Alluvial ridges form over centuries to millennia (Kiss et al., 2022) and represent the time-integrated deposition of channel belt dynamics; an amalgam of levee, crevasse splay, and bar deposits that grows through channel migration and overbank deposition (Figure 1a) (Allen, 1965; Bridge, 1984; Slingerland & Smith, 1998; Swartz et al., 2022). Even though alluvial ridges are connected to avulsion, their prevalence and character along river courses is rarely mapped. Rivers in tectonically subsiding basins or near the coast produce alluvial ridges (Fisk, 1944; Hassenruck-Gudipati et al., 2022; Piovan et al., 2012; Wu et al., 2023), but no large-scale census of the landform exists. The best records of modern alluvial ridge occurrence come from well-documented case studies, such as the Mississippi River, and from archeological literature, as ancient communities often inhabited ridges (Kidder & Liu, 2017).

However, records of alluvial ridges are spatially limited and there are still basic unanswered questions about their spatial distribution. For instance on an avulsing river are alluvial ridges found everywhere or only in discrete locations? If they are discrete features, then mapping and measuring alluvial ridges could serve as useful precursors to avulsion activity. Recent work suggests that avulsion potential (Λ), which combines the height and

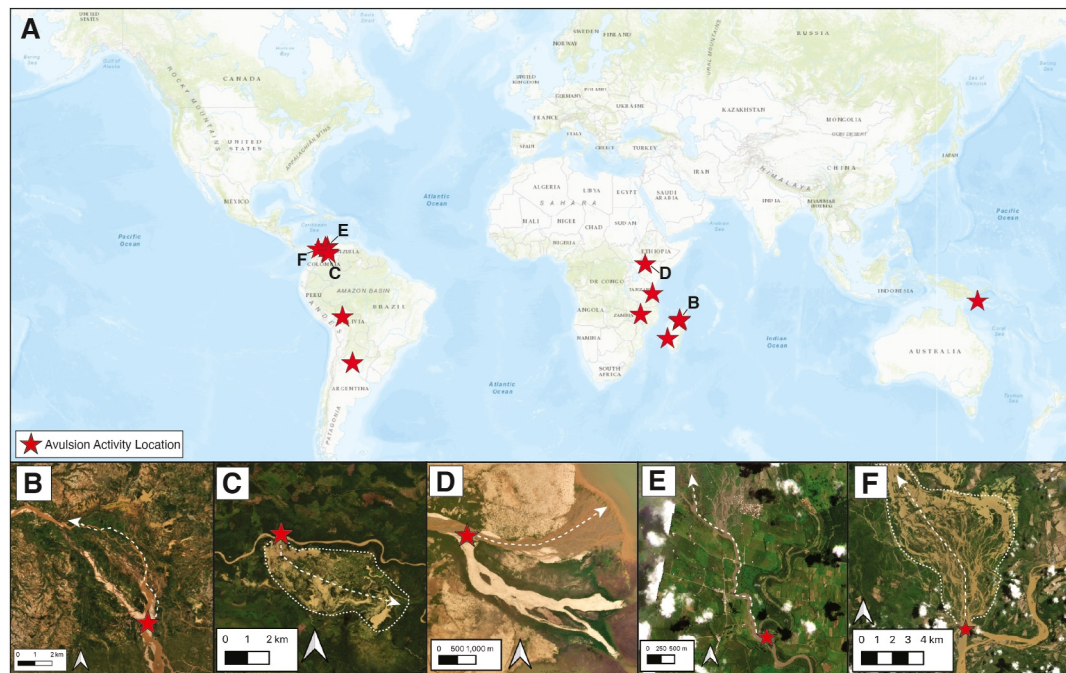


Figure 1. (a) Global distribution of 14 rivers analyzed in this study that exhibited recent avulsion activity. (b) Anjobony River, Madagascar: avulsion (2018). (c) Río Sarare, Venezuela: Progradational splay (2023). (d) Turkwel River, Kenya: delta avulsion (2019). (e) Río Chama, Venezuela: Progradational splay damaging the town of La Fortuna (2022). (e) Río Cauca, Colombia: progradational crevasse splay (2021).

slope of alluvial ridges relative to the channel, can predict avulsion occurrence (Gearon et al., 2024). Given that avulsion frequency and location are expected to change in a warming climate (Chadwick et al., 2020) and avulsions disproportionately occur in the Global South (Gearon et al., 2024), we need models to explain their location and impact.

Here we investigate the spatial structure of alluvial ridges along avulsing rivers. We selected 14 rivers where we have pre-avulsion topography and distributed cross-sections downstream to calculate Λ every 200 m. With these data, we test the hypothesis that the spatial structure of Λ along a river defines segments of enhanced avulsion potential.

2. Quantifying Avulsion Potential

Since early pioneering work, it has been accepted that rivers generate alluvial ridges prior to avulsion (Allen, 1965; Fisk, 1944). Ridges are created because higher sedimentation near the channel belt compared to the floodplain builds positive topography over time (Mohrig et al., 2000; Pizzuto, 1987). Two metrics have traditionally quantified ridge geometry: superelevation (β), the ratio of ridge height (H_{AR}) to channel depth (H_M), and gradient advantage (γ), the ratio of ridge slope (S_{AR}) to channel slope (S_M).

While these metrics are widely used in numerical models to predict avulsions (Hajek & Wolinsky, 2012), neither is universally predictive. For example, the Mississippi River exhibits levee slopes up to ~ 100 x steeper than the channel bed slope in multiple locations without evidence of avulsion (Aslan et al., 2005). A recent remote sensing study (Gearon et al., 2024) proposed that avulsions occur when alternative floodplain paths have a shear stress advantage over the current path. When formulated this way, the ratio expressing the relative shear stress between an alternate path and the main channel simplifies to $\beta\gamma$ and the avulsion potential Λ is given as:

$$\frac{H_{AR}S_{AR}}{H_MS_M} = \beta\gamma \quad (1)$$

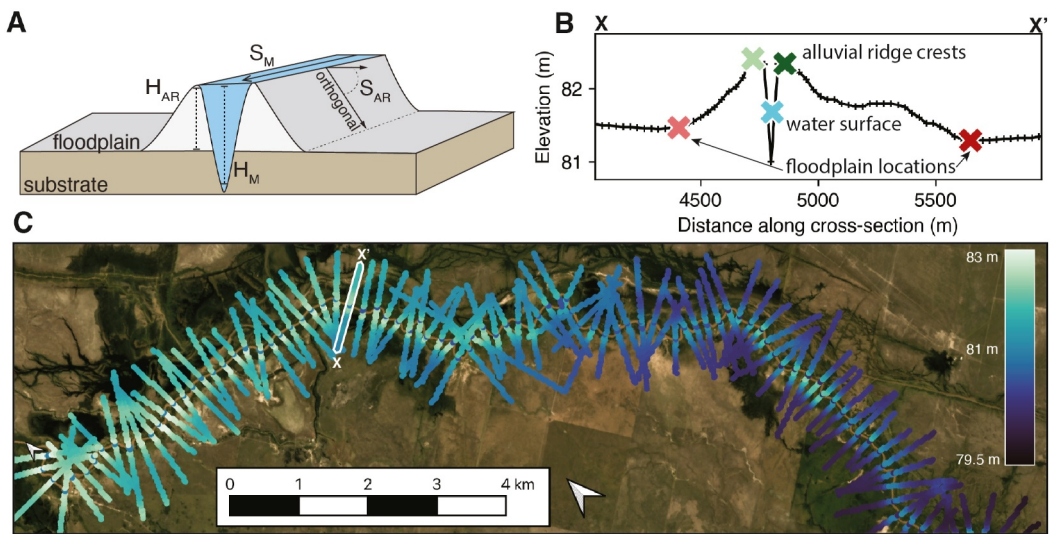


Figure 2. (a) Alluvial ridge schematic with key geometric labels; the height of the alluvial ridge (H_{AR}) above the floodplain, the slope of the alluvial ridge orthogonal to channel flow direction (S_{AR}), the depth of the channel (H_M), and the slope of the channel bed (S_M), here represented as the water surface slope due under a steady-state flow assumption. (b) Topographic section from FABDEM of the Río Utis ($-29.634, -62.881$ WGS84) illustrating typical alluvial ridge topography with labeled measurements. Water surface elevations were measured with ICESat-2. (c) Map view of Río Utis showing FABDEM-sampled cross-sections, perpendicular to flow, with the ~ 200 m original node spacing.

This relationship suggests β and γ are inversely related when rivers avulse, and the field data from 58 rivers quantifies the threshold for avulsion at a median value of $\Lambda \approx 2$ (Gearon et al., 2024). However, these values of Λ were only measured at each avulsion site. To determine if Λ is a viable precursor to avulsion we must quantify how Λ varies along rivers in context of avulsion activity.

3. Methods

3.1. Topographic Measurements

We measured β , γ , and calculated Λ using digital elevation models (DEMs) for 14 rivers that have experienced avulsion activity (Figure 1). We limited our analysis to these rivers because they experienced avulsion activity contemporary to, or post-DEM acquisition, which ensures the topography is not affected by the avulsion-related deposition. Avulsion activity is defined as evidence of avulsion completion (Figures 1b and 1d) or initiation, including crevassing (Figures 1c, 1e, and 1f, Tables S1 and S2). Our selection spans diverse source-to-sink settings: fans ($n = 3$), floodplains ($n = 9$), and deltas ($n = 2$) and contains a total of 37 instances of avulsion activity.

For each river, we generated cross-sections every 200 m along the centerline using the SWOT River Database (SWORD) (Altenau et al., 2021) and FABDEM (Hawker et al., 2022) (Figure 2). Channel-perpendicular cross-sections extended 200 times the local channel width, and for channels more than 250 m wide we used 50 times the width. The cross-sections started at major tributaries, distributaries, or mountain fronts and continued downstream until encountering another channel or local water body. On each cross section, we identified alluvial ridge crests as the tallest near-channel topography (within ~ 10 channel widths) with positive curvature, and floodplain elevations as adjacent locations with distinct slope breaks (Figures 2a and 2b). We calculated H_{AR} as the elevation difference between the ridge crest and floodplain, S_{AR} as H_{AR} divided by intervening distance, and obtained S_M from SWORD. H_M was estimated using the Boost-Assisted Stream Estimator for Depth, a hydraulic-geometry informed machine learning model incorporating river width, slope, and discharge data (Gearon et al., 2024) (see Supplement for details and caveats associated with measurements).

3.2. Avulsion Activity Length

One measure of avulsion activity size and impact is the planform extent of the avulsion channel or progradational splay (Figures 1b–1f, Figures S3–S16 in Supporting Information S1). Longer avulsions have a greater impact on the surrounding hydrology and ecology and probably are associated with larger floods. We measured the avulsion activity length (L_A) as the distance along the avulsion-channel-belt centerline from take-off location to rejoining point or termination in a local water body or delta (dashed lines in Figures 1b–1f). While each of the 14 rivers contain multiple instances of avulsion activity, we only measured the length of the avulsion activity that occurred closest in time to the DEM acquisition to ensure the least amount of morphodynamic reworking. For ongoing avulsions with splays, we used the planform extent of the splay's centerline as a minimum L_A estimate. For the two delta avulsions in our study, we also calculated the backwater length (L_B) by dividing H_M by channel slope for datapoints within 20% of the distance to the shoreline relative to the entire transport length, as backwater lengths typically scale with avulsion lengths in deltaic systems and thus provides an independent check on our L_A measurements.

3.3. Spatial Analysis

The unidirectional flow of rivers creates inherent connectivity, as upstream conditions directly influence downstream characteristics, leading to spatial autocorrelation. Examining this autocorrelation in Λ defines the spatial scale over which its structure remains consistent and may indicate regions of enhanced avulsion potential. To quantify the spatial structure of the Λ series, we employed semivariograms, wavelets, and Local Indicators of Spatial Association (LISA) analyses (Anselin, 1995). Following Robert (1988), we fit experimental semivariograms with a combined model containing an exponential and two periodic components (see Text S7 in Supporting Information S1 for full details). The model optimizes nine parameters through a two-stage fitting process: a nugget (c_0), partial sill (c), and range parameter (r) for the exponential component, and amplitude and wavelength parameters (a_i, b_i, l_i) for each periodic component. From these, we derive two key length scales: $L_C = 3r$, the effective range or characteristic lag distance over which Λ values are correlated, and $L_\lambda = l_1$, the primary wavelength of the dominant periodic component. While the model includes a second periodic component, following Robert (1988), we focus on L_λ as higher harmonics typically do not represent physically meaningful patterns in geomorphic systems.

To pinpoint the high- Λ zones within the reach, we used LISA analysis which classifies locations into four categories based on their value relative to neighboring points: “high-high” clusters where elevated Λ values are surrounded by other high values, “low-high” and “high-low” transitions where high values border areas of lower Λ (or vice versa), and “low-low” clusters of consistently low values (See Text S8 in Supporting Information S1 for details). We smoothed the Λ data using a Savitzky-Golay filter with a window of length L_C to reduce noise while maintaining spatial correlation at the L_C scale. We then recorded the number of avulsion activity events that corresponded to regions of high-high Λ clusters surrounded by low-high clusters. We also implemented a proximity-weighted analysis by comparing the distribution of Λ values within one correlation length (L_C) upstream and downstream of avulsion activity locations to distinguish between these populations and weighting the analysis inversely by the number of cross-sections per river.

4. Results

4.1. Downstream Patterns in Λ

The spatial structure of Λ suggests that alluvial ridges are not ubiquitous along river reaches but form over distinct spatial scales (Figures 3a, 3b, and 3f; Figures S3–S16 in Supporting Information S1). Most rivers exhibit a first-order trend of increasing Λ downstream, with multiple scales of superimposed, higher-order fluctuations that vary over one to two orders of magnitude. Proximity-weighted analysis incorporating all instances of avulsion activity ($n = 37$) across our 14 rivers shows that typically $\Lambda > 2$ near avulsion activity sites but remains below 2 elsewhere (Figure 4a), supporting the hypothesis that taller and steeper alluvial ridges only form in certain locations along the river and are precursors to river avulsion (Gearon et al., 2024). The LISA analysis provides independent confirmation; 73% of all avulsion activity events are associated with significant “hot-spots” or regions of high-high clusters where the magnitude of Λ is significantly larger than neighboring points ($p = 0.05$, Figure 3b, Figures S3–S16 in Supporting Information S1).

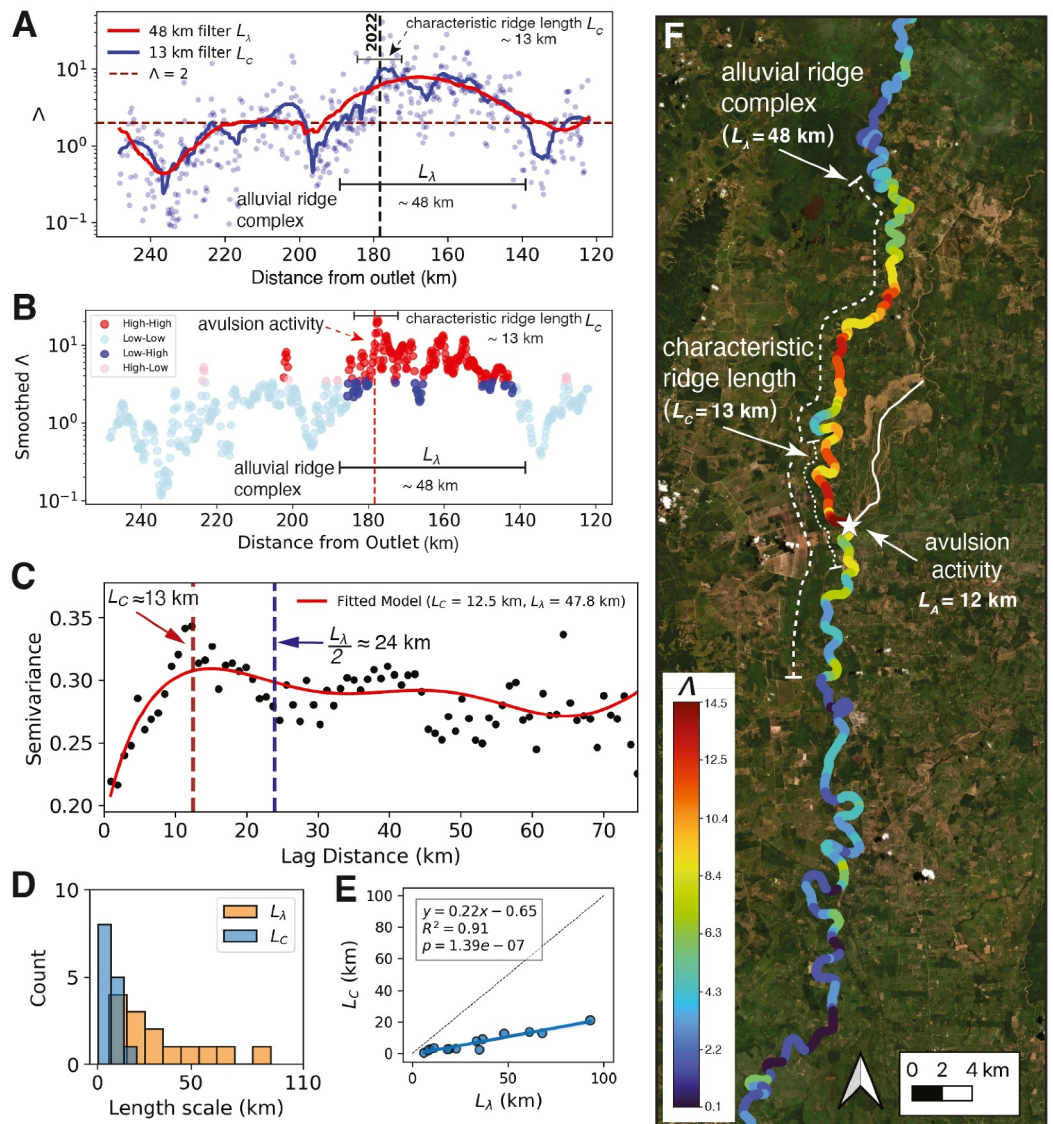


Figure 3. (a) Downstream changes in Λ on Río Zulia, Venezuela display two characteristic scales of alluvial ridge geometry (L_λ and L_c), shown here with Savitzky-Golay filters. (b) Local Indicators of Spatial Association analysis of smoothed Λ demonstrating avulsion activity coincides with “high-high” zones ($p = 0.05$). (c) Experimental semivariogram calculated from Λ data in panel (a) with fitted theoretical semivariogram model and lengthscales L_c and L_λ . To avoid edge effects, semivariograms are only calculated for half the domain length, hence maximum lag distance is shorter than total length of river reach (see panel A) and we plot $L_\lambda/2$ for visualization. (d) L_λ ranges from 8 to 83 km (25–1,700 channel widths) with $\bar{L}_\lambda = 30 \text{ km}$ (350 channel widths). L_c ranges from 1.4 to 31 km (5–630 channel widths) with $\bar{L}_c = 8 \text{ km}$ (e) Regression between L_λ and L_c . (f) Map view of Río Zulia, Venezuela: progradational splay (2022). Avulsion activity location is denoted with a star. The length of the splay approximates L_c . Λ is smoothed using a rolling average scaled to median meander length, with color range set to 2nd–98th percentiles for visualization.

4.2. Characteristic Length Scales of Alluvial Ridge Systems

Looking at the downstream changes in Λ , we identify two dominant alluvial ridge length scales from semivariogram analysis (Figures 3a and 3c). Across these 14 river and 37 instances of avulsion activity, L_c is consistently one-third the length of L_λ (Figures 3d and 3e). In all cases, $L_c < L_\lambda$ on a given river, indicating a nested hierarchy of scales (Figures 3d and 3e). The longer L_λ is composed of multiple segments of L_c (See “low-high” blue points separating zones of red “high-high” points in Figure 3b). Nondimensionally, L_c is on average 100 channel widths ($L_c \approx 8 \text{ km}$) and L_λ is on average 350 channels widths ($L_\lambda \approx 30 \text{ km}$).

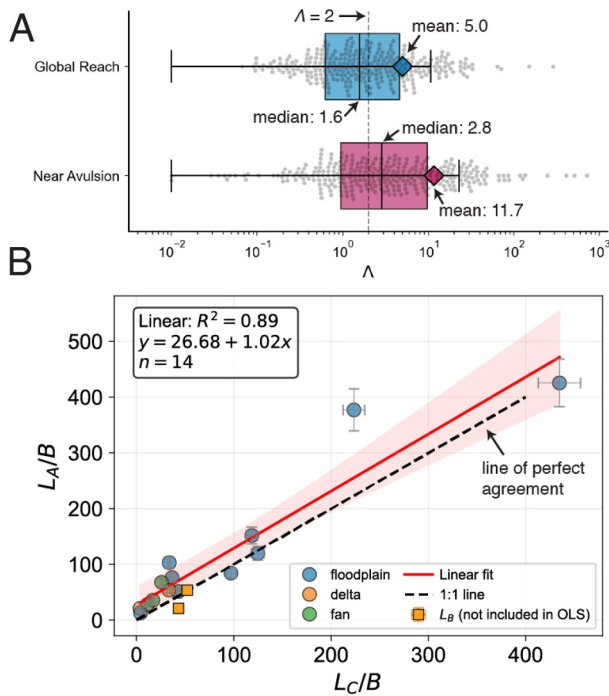


Figure 4. (a) Values of Λ within a $\pm L_c$ window of each avulsion activity site (Near Avulsion) are 75% larger than randomly selected Λ values outside of $\pm L_c$ (Global Reach). Diamonds represent weighted mean Λ . Λ values were inversely weighted according to river sample size, ensuring a valid comparison, $n = 1,948$ for each group (b) Avulsion activity length (L_A) normalized by channel width (B) scales with the characteristic correlation length of avulsion potential Λ (L_c), also normalized by B , $n = 14$. For the two delta avulsions (Lilongwe and Turkwel Rivers), backwater length scales (L_B) are shown to highlight their similarity to L_c , but are not included in the regression.

systems (Jerolmack & Mohrig, 2007). These shorter L_c segments span multiple meander wavelengths and possibly could form through channel migration and overbank deposition. An alternative explanation is that both scales could emerge from a single process; L_λ could emerge through the amalgamation of multiple generations of L_c segments. This is conceivable if initial avulsions concentrate future activity as has been observed in reduced-complexity models (Martin & Edmonds, 2022, 2023).

5.2. Predicting Avulsion Activity Size and Impact

An important open question is what sets the size and impact of river avulsions. While this topic has been investigated in deltaic settings (Brooke et al., 2022; Chadwick et al., 2020; Ganti et al., 2016), there are no field-tested theories for avulsion size scaling in fans and floodplains. An initial conjecture might be that avulsion activity size scales with Λ , but using L_A (the centerline distance along the avulsion channel belt) as a measure of size and impact, shows no relationship ($R^2 = 0.06$). Early ideas about alluvial ridges suggested that their positive topography “pushes” away advancing avulsion channels, prohibiting reoccupation until ridge topography becomes surmountable by pathfinding avulsion flows (Allen, 1978; Bridge & Leeder, 1979; Edmonds et al., 2016; Martin & Edmonds, 2022).

Our data provide empirical support for this “ridge push” mechanism. Alluvial ridges are precursors to river avulsion activity (Figure 4a), and because L_c represents the characteristic length over which ridge geometry remains correlated, L_A should be related to L_c . Our data confirm this, showing L_A scales linearly with L_c across geomorphic landforms, from fans to deltas ($R^2 = 0.89$, $p = 6.03 \times 10^{-7}$) (Figure 4b). The one-to-one relationship suggests that avulsion channels are pushed away from the parent channel by the positive topography of the alluvial ridge until rejoining the main channel becomes possible, likely by exploiting intra-complex low spots

Neither length scale correlates with channel properties like discharge, width, or meander wavelength (Figure S1 in Supporting Information S1). Both scales have weak negative correlation with slope, which is unsurprising given channel slope appears in Λ (Equation 1). To ensure that L_λ is not a model artifact, we performed wavelet analysis on the raw Λ data and found the dominant wavelength of the wavelet power spectrum (λ_w) correlates with L_λ (See Text S9 and Figure S2 in Supporting Information S1; $R^2 = 0.86$, $p < .001$).

5. Discussion

5.1. Formation Mechanisms of Ridge Scales

Our analysis of the spatial structure of Λ on avulsing rivers reveals two key spatial scales of alluvial ridge geometry, L_c and L_λ . We interpret these length scales to correspond to alluvial ridge segments of characteristic length L_c that amalgamate to form a higher-order alluvial ridge complex of characteristic length L_λ (Figures 3a and 3b). Within a complex, alluvial ridges are neither continuous nor uniform. This discontinuous nature is consistent with observations of levee formation and overbank deposition, which are notoriously sporadic (Hassenruck-Gudipati et al., 2022; Johnston et al., 2019).

These length scales likely form through distinct mechanisms. The larger-scale L_λ is not related to channel properties (Figure S1 in Supporting Information S1), and instead could form when rivers aggrade their beds and banks in response to changing boundary conditions. Using typical diffusivities of $0.01\text{--}0.1 \text{ km}^2/\text{yr}$ for gravel and sand respectively (Marr et al., 2000; Paola et al., 1992), and the diffusive scaling relationship $L = \sqrt{\kappa t}$ where κ is diffusivity and t is time, L_λ would require 9,000–90,000 years to form, consistent with fluctuations in incoming sediment supply or changes in discharge related to climatic oscillations (Nicholas et al., 1995; Paola et al., 1992). In contrast, the smaller-scale L_c would develop over just 640–6,400 years, consistent with avulsion frequency estimates in natural sys-

tems (Jerolmack & Mohrig, 2007). These shorter L_c segments span multiple meander wavelengths and possibly could form through channel migration and overbank deposition. An alternative explanation is that both scales could emerge from a single process; L_λ could emerge through the amalgamation of multiple generations of L_c segments. This is conceivable if initial avulsions concentrate future activity as has been observed in reduced-complexity models (Martin & Edmonds, 2022, 2023).

(e.g., blue points surrounded by red in Figure 3b, Figures S3–S16 in Supporting Information S1). This is consistent with cellular model predictions of avulsion pathfinding (Martin & Edmonds, 2022, 2023).

Previous work in deltas shows L_A scales with the backwater length L_B (Brooke et al., 2022). In our limited deltaic cases ($n = 2$), we find that $L_B \approx L_C$, suggesting alluvial ridge size may approach the backwater length scale. This is possible because channel migration is reduced in the backwater zone (Wu et al., 2023) and levees and ridges are more prevalent and continuous (Hassenruck-Gudipati et al., 2022; Swartz et al., 2022). However, given the small number of deltaic avulsions in our database, the connection between L_B and L_C is unknown, and L_B likely remains more predictive of deltaic L_A as it directly incorporates hydrodynamics (Brooke et al., 2022; Ganti et al., 2016).

5.3. Implications for Avulsion Hazard Assessment

Our analysis shows that alluvial ridges are not ubiquitous features along avulsing rivers and therefore mapping their presence and size should serve as a useful way to predict avulsion activity and size (Figure 4). These results pave the way for creating global avulsion risk maps. Avulsion hazards remain invisible because most flood models do not include erosion and deposition—a critical gap for communities in the Global South, where avulsions occur disproportionately (Gearon et al., 2024). By measuring and monitoring Λ values through readily available topographic data and standard GIS tools, practitioners can identify discrete areas with heightened avulsion activity risk ($\Lambda \geq 2$). Integrating these results with a probabilistic model of avulsion pathfinding (Gearon et al., 2024) can define hazards corridors in the floodplain. L_C provides a downstream minimum extent for potential impact zones, while L_λ spacing between high and low zones helps predict the likely extent of successive avulsion-prone reaches. Importantly, this approach requires only periodic, targeted topographic surveys rather than extensive hydrologic and morphodynamic monitoring, making it particularly valuable for regions with limited resources or instrumentation.

The framework we present is, in principle, scale-independent, though our analysis currently focuses on larger rivers due to SWORD and FABDEM resolution constraints. As global topographic data sets improve in resolution and temporal coverage, this approach can help identify avulsion hazards across a broader spectrum of river systems, expanding its utility for risk assessment and planning.

Notation

L_A	Avulsion activity length (km)
L_B	Backwater length (km)
H_{AR}	Alluvial ridge height (m)
H_M	Channel depth (m)
S_{AR}	Alluvial ridge slope (m/m)
S_M	Channel slope (m/m)
β	Superelevation: Ratio of alluvial ridge height (H_{AR}) to channel depth (H_M)
γ	Gradient advantage: Ratio of alluvial ridge slope (S_{AR}) to channel slope (S_M)
Λ	Avulsion potential (dimensionless)
L_C	Characteristic length scale of alluvial ridge segments (km)
L_λ	Characteristic length scale of alluvial ridge complexes (km)
λ_w	Dominant wavelength from wavelet analysis (km)
h	Lag distance in semivariogram (km)
c	Partial sill of semivariogram (—)
r	Range parameter of semivariogram (km)
a_i, b_i	Amplitude parameters of semivariogram's periodic component (—)

l_i	Wavelength parameters of semivariogram's periodic component (km)
c_0	Nugget variance in semivariogram
$\gamma(h)$	Semivariance at lag distance h
$\gamma_1(h)$	Exponential component of the semivariogram: $c[1 - \exp(-h/r)]$
$\gamma_2(h)$	Periodic component of the semivariogram: $\sum_i [a_i \cos(2\pi h/l_i) + b_i \sin(2\pi h/l_i)]$
n	Sample number
R^2	Coefficient of determination
p	p-value

Data Availability Statement

The river cross section data and analysis code used in the study are available on Zenodo via <https://doi.org/10.5281/zenodo.14895103> with an MIT License (Gearon, 2025).

Acknowledgments

Planet Labs PBC for optical imagery. Curt Cignetti for inspiration. DAE and JHG were supported by grants from the National Science Foundation: 2321056 and 2436929.

References

- Allen, J. R. L. (1965). A review of the origin and characteristics of recent alluvial sediments. *Sedimentology*, 5(2), 89–191. <https://doi.org/10.1111/j.1365-3091.1965.tb01561.x>
- Allen, J. R. L. (1978). Studies in fluvialite sedimentation: An exploratory quantitative model for the architecture of avulsion-controlled alluvial suites. *Sedimentary Geology*, 21(2), 129–147. [https://doi.org/10.1016/0037-0738\(78\)90002-7](https://doi.org/10.1016/0037-0738(78)90002-7)
- Altenau, E. H., Pavelsky, T. M., Durand, M. T., Yang, X., Frasson, R. P. d. M., & Bendezu, L. (2021). The Surface Water and Ocean Topography (SWOT) Mission River Database (SWORD): A global river network for satellite data products. *Water Resources Research*, 57(7). <https://doi.org/10.1029/2021WR030054>
- Anselin, L. (1995). Local indicators of spatial association—LISA. *Geographical Analysis*, 27(2), 93–115. <https://doi.org/10.1111/j.1538-4632.1995.tb00338.x>
- Aslan, A., Autin, W. J., & Blum, M. D. (2005). Causes of river avulsion: Insights from the Late Holocene avulsion history of the Mississippi River. *U.S.A. Journal of Sedimentary Research*, 75(4), 650–664. <https://doi.org/10.2110/jsr.2005.053>
- Bridge, J. S. (1984). Large-scale facies sequences in alluvial overbank environments. *Journal of Sedimentary Research*, 54(2), 583–588. <https://doi.org/10.1306/212F8477-2B24-11D7-8648000102C1865D>
- Bridge, J. S., & Leeder, M. R. (1979). A simulation model of alluvial stratigraphy. *Sedimentology*, 26(5), 617–644. <https://doi.org/10.1111/j.1365-3091.1979.tb00935.x>
- Brooke, S., Chadwick, A. J., Silvestre, J., Lamb, M. P., Edmonds, D. A., & Ganti, V. (2022). Where rivers jump course. *Science*, 376(6596), 987–990. <https://doi.org/10.1126/science.abm1215>
- Chadwick, A. J., Lamb, M. P., & Ganti, V. (2020). Accelerated river avulsion frequency on lowland deltas due to sea-level rise. *Proceedings of the National Academy of Sciences of the United States of America*, 117(30), 17584–17590. <https://doi.org/10.1073/pnas.1912351117>
- Edmonds, D. A., Hajek, E., Downton, N., & Bryk, A. B. (2016). Avulsion flow-path selection on rivers in foreland basins. *Geology*, 44(9), 695–698. <https://doi.org/10.1130/g38082.1>
- Fisk, H. N. (1944). *Geological investigation of the alluvial valley of the lower Mississippi River: U.S. Department of the Army, Mississippi River Commission, 78p* (Tech. Rep.). War Department, Corps of Engineers, Navy.
- Ganti, V., Chadwick, A. J., Hassenruck-Gudipati, H. J., & Lamb, M. P. (2016). Avulsion cycles and their stratigraphic signature on an experimental backwater-controlled delta. *Journal of Geophysical Research: Earth Surface*, 121(9), 1651–1675. <https://doi.org/10.1002/2016JF003915>
- Gearon, J. H. (2025). *jameshgrn/avulsionprecursors: Zenodo archive (first)*. Zenodo. <https://doi.org/10.5281/zenodo.14895103>
- Gearon, J. H., Martin, H. K., DeLisle, C., Barefoot, E. A., Mohrig, D., Paola, C., & Edmonds, D. A. (2024). Rules of river avulsion change downstream. *Nature*, 634(8032), 91–95. <https://doi.org/10.1038/s41586-024-07964-2>
- Hajek, E. A., & Wolinsky, M. A. (2012). Simplified process modeling of river avulsion and alluvial architecture: Connecting models and field data. *Sedimentary Geology*, 257–260, 1–30. <https://doi.org/10.1016/j.sedgeo.2011.09.005>
- Hassenruck-Gudipati, H. J., Passalacqua, P., & Mohrig, D. (2022). Natural levees increase in prevalence in the backwater zone: Coastal Trinity River, Texas, USA. *Geology*, 50(9), 1068–1072. <https://doi.org/10.1130/G50011.1>
- Hawker, L., Uhe, P., Paulo, L., Sosa, J., Savage, J., Sampson, C., & Neal, J. (2022). A 30 m global map of elevation with forests and buildings removed. *Environmental Research Letters*, 17(2), 024016. <https://doi.org/10.1088/1748-9326/ac4d4f>
- Jerolmack, D. J., & Mohrig, D. (2007). Conditions for branching in depositional rivers. *Geology*, 35(5), 463. <https://doi.org/10.1130/g23308a.1>
- Johnston, G. H., David, S. R., & Edmonds, D. A. (2019). Connecting fluvial levee deposition to flood-basin hydrology. *Journal of Geophysical Research: Earth Surface*, 124(7), 1996–2012. <https://doi.org/10.1029/2019JF005014>
- Kidder, T. R., & Liu, H. (2017). Bridging theoretical gaps in geoarchaeology: Archaeology, geoarchaeology, and history in the Yellow River valley, China. *Archaeological and Anthropological Sciences*, 9(8), 1585–1602. <https://doi.org/10.1007/s12520-014-0184-5>
- Kiss, T., Sipos, G., & Vass, R. (2022). Alluvial ridge development and structure: Case study on the Upper Tisza, Hungary. *Geographica Panonica*, 26(3), 230–240. <https://doi.org/10.5937/gp26-38365>
- Marr, J. G., Swenson, J. B., Paola, C., & Voller, V. R. (2000). A two-diffusion model of fluvial stratigraphy in closed depositional basins. *Basin Research*, 12(3–4), 381–398. <https://doi.org/10.1111/j.1365-2117.2000.00134.x>

- Martin, H. K., & Edmonds, D. A. (2022). The push and pull of abandoned channels: How floodplain processes and healing affect avulsion dynamics and alluvial landscape evolution in foreland basins. *Earth Surface Dynamics*, 10(3), 555–579. <https://doi.org/10.5194/esurf-10-555-2022>
- Martin, H. K., & Edmonds, D. A. (2023). Avulsion dynamics determine fluvial fan morphology in a cellular model. *Geology*, 51(8), 796–800. <https://doi.org/10.1130/G51138.1>
- Mohrig, D., Heller, P. L., Paola, C., & Lyons, W. J. (2000). Interpreting avulsion process from ancient alluvial sequences: Guadalupe-Matarranya system (northern Spain) and Wasatch Formation (western Colorado). *GSA Bulletin*, 112(12), 1787–1803. [https://doi.org/10.1130/0016-7606\(2000\)112<1787:IAPFAA>2.0.CO;2](https://doi.org/10.1130/0016-7606(2000)112<1787:IAPFAA>2.0.CO;2)
- Nicholas, A., Aalto, R., Sambrook Smith, G., & Schwendel, A. (2018). Hydrodynamic controls on alluvial ridge construction and avulsion likelihood in meandering river floodplains. *Geology*, 46(7), 639–642. <https://doi.org/10.1130/G40104.1>
- Nicholas, A., Ashworth, P., Kirkby, M., Macklin, M., & Murray, T. (1995). Sediment slugs: Large-scale fluctuations in fluvial sediment transport rates and storage volumes. *Progress in Physical Geography: Earth and Environment*, 19(4), 500–519. <https://doi.org/10.1177/03091339501900404>
- Paola, C., Heller, P. L., & Angevine, C. L. (1992). The large-scale dynamics of grain-size variation in alluvial basins, 1: Theory. *Basin Research*, 4(2), 73–90. <https://doi.org/10.1111/j.1365-2117.1992.tb00145.x>
- Piovan, S., Mozzi, P., & Zecchin, M. (2012). The interplay between adjacent Adige and Po alluvial systems and deltas in the late Holocene (Northern Italy). *Géomorphologie: Relief, Processus, Environnement*, 2012(4), 427–440. <https://doi.org/10.4000/gemorphologie.10034>
- Pizzuto, J. E. (1987). Sediment diffusion during overbank flows. *Sedimentology*, 34(2), 301–317. <https://doi.org/10.1111/j.1365-3091.1987.tb00779.x>
- Robert, A. (1988). Statistical properties of sediment bed profiles in alluvial channels. *Mathematical Geology*, 20(3), 205–225. <https://doi.org/10.1007/BF00890254>
- Sinha, R. (2009). The Great avulsion of Kosi on 18 August 2008. *Current Science*, 97, 429–433.
- Slingerland, R., & Smith, N. D. (1998). Necessary conditions for a meandering-river avulsion. *Geology*, 26(5), 435–438. [https://doi.org/10.1130/0091-7613\(1998\)026<0435:NCFAMR>2.3.CO;2](https://doi.org/10.1130/0091-7613(1998)026<0435:NCFAMR>2.3.CO;2)
- Swartz, J. M., Cardenas, B. T., Mohrig, D., & Passalacqua, P. (2022). Tributary channel networks formed by depositional processes. *Nature Geoscience*, 15(3), 216–221. <https://doi.org/10.1038/s41561-022-00900-x>
- Wu, C., Kim, W., Herring, R., Cardenas, B. T., Dong, T. Y., Ma, H., et al. (2023). Lowland river sinuosity on Earth and Mars set by the pace of meandering and avulsion. *Nature Geoscience*, 16(8), 747–753. <https://doi.org/10.1038/s41561-023-01231-1>

References From the Supporting Information

- Dandabathula, G., Hari, R., Ghosh, K., Bera, A. K., & Srivastav, S. K. (2023). Accuracy assessment of digital bare-earth model using ICESat-2 photons: Analysis of the FABDEM. *Modeling Earth Systems and Environment*, 9(2), 2677–2694. <https://doi.org/10.1007/s40808-022-01648-4>
- Deal, E. (2021). Downstream hydraulic geometry data compilation. Retrieved from <https://www.hydroshare.org/resource/0629ffb81fdb40aa9e6be42cc11918ca/>:CUAHSIHydroShare
- Dunne, K. B. J., & Jerolmack, D. J. (2018). Evidence of, and a proposed explanation for, bimodal transport states in alluvial rivers. *Earth Surface Dynamics*, 6(3), 583–594. <https://doi.org/10.5194/esurf-6-583-2018>
- Edmonds, D. A., Martin, H. K., Valenza, J. M., Henson, R., Weissmann, G. S., Miltenberger, K., et al. (2021). Rivers in reverse: Upstream-migrating dechannelization and flooding cause avulsions on fluvial fans. *Geology*, 50(1), 37–41. <https://doi.org/10.1130/G49318.1>
- Fahrlund, E. (2022). Copernicus DEM product handbook (public document no. AO-1/9422/18/I-LG). *Airbus*.
- Lechner, B., & Grill, G. (2013). Global river hydrography and network routing: Baseline data and new approaches to study the world's large river systems. *Hydrological Processes*, 27(15), 2171–2186. <https://doi.org/10.1002/hyp.9740>
- Matheron, G. (1965). *Les Variables Régionalisées Et Leur Estimation: Une Application De La Théorie De Fonctions Aléatoires Aux Sciences De La Nature*. Masson et Cie.
- Müller Schmied, H., Cáceres, D., Eisner, S., Flörke, M., Herbert, C., Niemann, C., et al. (2021). The global water resources and use model WaterGAP v2.2d: Model description and evaluation. *Geoscientific Model Development*, 14(2), 1037–1079. <https://doi.org/10.5194/gmd-14-1037-2021>
- Neuenschwander, A. L., Pitts, K. L., Jolley, B. P., Robbins, J., Klotz, B., Popescu, S. C., et al. (2023). ATLAS/ICESat-2 L3A land and vegetation height, version 6. NASA National Snow and Ice Data Center Distributed Active Archive Center. <https://doi.org/10.5067/ATLAS/ATL08.006>
- Seeger, K., Minderhoud, P. S. J., Peffeköver, A., Vogel, A., Brückner, H., Kraas, F., & Brill, D. (2023). Assessing land elevation in the Ayeyarwady Delta (Myanmar) and its relevance for studying sea level rise and delta flooding. *Hydrology and Earth System Sciences*, 27(11), 2257–2281. <https://doi.org/10.5194/hess-27-2257-2023>
- Soergel, U., Jacobsen, K., & Schack, L. (2013). The TanDEM-X mission: Data collection and deliverables.
- Trampush, S. M., Huzurbazar, S., & McElroy, B. (2014). Empirical assessment of theory for bankfull characteristics of alluvial channels. *Water Resources Research*, 50(12), 9211–9220. <https://doi.org/10.1002/2014WR015597>
- Valenza, J. M., Edmonds, D. A., Hwang, T., & Roy, S. (2020). Downstream changes in river avulsion style are related to channel morphology. *Nature Communications*, 11(1), 2116. <https://doi.org/10.1038/s41467-020-15859-9>